

# We are IntechOpen, the world's leading publisher of Open Access books Built by scientists, for scientists

6,900

Open access books available

186,000

International authors and editors

200M

Downloads

Our authors are among the

154

Countries delivered to

TOP 1%

most cited scientists

12.2%

Contributors from top 500 universities



WEB OF SCIENCE™

Selection of our books indexed in the Book Citation Index  
in Web of Science™ Core Collection (BKCI)

Interested in publishing with us?  
Contact [book.department@intechopen.com](mailto:book.department@intechopen.com)

Numbers displayed above are based on latest data collected.  
For more information visit [www.intechopen.com](http://www.intechopen.com)



# Model Reference Adaptive Control for Robotic Manipulation with Kalman Active Observers

Rui Cortesão  
*Institute of Systems and Robotics, Electrical and Computer Engineering Department,  
University of Coimbra  
Portugal*

## 1. Introduction

Nowadays, the presence of robotics in human-oriented applications demands control paradigms to face partly known, unstructured and time-varying environments. Contact tasks and compliant motion strategies cannot be neglected in this scenario, enabling safe, rewarding and pleasant interactions. Force control, in its various forms, requires special attention, since the task constraints can change abruptly (e.g. free-space to contact transitions) entailing wide variations in system parameters. Modeling contact/non-contact states and designing appropriate controllers is yet an open problem, even though several control solutions have been proposed along the years. Two main directions can be followed, depending on the presence of force sensors. The perception of forces allows explicit force control (e.g. hybrid position/force control) to manage the interaction imposed by the environment, which is in general more accurate than implicit force control schemes (e.g. impedance control) that do not require force sensing. A major problem of force control design is the robustness to disturbances present in the robotic setup. In this context, disturbances include not only system and measurement noises but also parameter mismatches, nonlinear effects, discretization errors, couplings and so on. If the robot is interacting with unknown objects, "rigid" model based approaches are seldom efficient and the quality of interaction can be seriously deteriorated. Model reference adaptive control (MRAC) schemes can have an important role, imposing a desired closed loop behavior to the real plant in spite of modeling errors.

This chapter introduces the Active Observer (AOB) algorithm for robotic manipulation. The AOB reformulates the classical Kalman filter (CKF) to accomplish MRAC based on: 1) A desired closed loop system. 2) An extra equation to estimate an equivalent disturbance referred to the system input. An active state is introduced to compensate unmodeled terms, providing compensation actions. 3) Stochastic design of the Kalman matrices. In the AOB, MRAC is tuned by stochastic parameters and not by control parameters, which is not the approach of classical MRAC techniques. Robotic experiments will be presented, highlighting merits of the approach. The chapter is organized as follows: After the related work described in Section 3, the AOB concept is analyzed in Sections 4, 5 and 6, where the general algorithm and main design issues are addressed. Section 7 describes robotic

experiments. The execution of the peg-in-hole task with tight clearance is discussed. Section 8 concludes the chapter.

## 2. Keywords

Kalman Filter, State Space Control, Stochastic Estimation, Observers, Disturbances, Robot Force Control.

## 3. Related Work

Disturbance sources including external disturbances (e.g. applied external forces) and internal disturbances (e.g. higher order dynamics, nonlinearities and noise) are always present in complex control systems, having a key role in system performance. A great variety of methods and techniques have been proposed to deal with disturbances. De Schutter [Schutter, 1988] has proposed an extended deterministic observer to estimate the motion parameters of a moving object in a force control task. In [Chen et al., 2000], model uncertainties, nonlinearities and external disturbances are merged to one term and then compensated with a nonlinear disturbance observer based on the variable structure system theory. Several drawbacks of previous methods are also pointed out in [Chen et al., 2000]. The problem of disturbance decoupling is classical and occupies a central role in modern control theory. Many control problems including robust control, decentralized control and model reference control can be recast as an almost disturbance decoupling problem. The literature is very extensive on this topic. To tackle the disturbance decoupling problem, PID-based techniques [Estrada & Malabre, 1999], state feedback [Chu & Mehrmann, 2000] geometric concepts [Commault et al., 1997], tracking schemes [Chen et al., 2002] and observer techniques [Oda, 2001] have been proposed among others. In [Petersen et al., 2000], linear quadratic Gaussian (LQG) techniques are applied to uncertain systems described by a nominal system driven by a stochastic process. Safanov and Athans [Safanov & Athans, 1977] proofed how the multi-variable LQG design can satisfy constraints requiring a system to be robust against variations in its open loop dynamics. However, LQG techniques have no guaranteed stability margins [Doyle, 1978], hence Doyle and Stein have used fictitious noise adjustment to improve relative stability [Doyle & Stein, 1979].

In the AOB, the disturbance estimation is modeled as an auto-regressive (AR) process with fixed parameters driven by a random source. This process represents stochastic evolutions. The AOB provides a methodology to achieve model-reference adaptive control through extra states and stochastic design in the framework of Kalman filters.

It has been applied in several robotic applications, such as autonomous compliant motion of robotic manipulators [Cortês et al., 2000], [Cortês et al., 2001], [Park et al., 2004], haptic manipulation [Cortês et al., 2006], humanoids [Park & Khatib, 2005], and mobile systems [Coelho & Nunes, 2005], [Bajcinca et al., 2005], [Cortês & Bajcinca, 2004], [Maia et al., 2003].

## 4. AOB Structure

Given a discretized system with equations

$$x_{r,k} = \Phi_r x_{r,k-1} + \Gamma_r u_{k-1} + \xi_{x_{r,k}} \quad (1)$$

and

$$y_k = C_r x_{r,k} + \eta_k, \quad (2)$$

an observer of the state  $x_{r,k}$ ,  $\hat{x}_{r,k}$ , can be written as

$$\hat{x}_{r,k} = \Phi_{r,n} \hat{x}_{r,k-1} + \Gamma_{r,n} u_{k-1} + K_k [y_k - C_r (\Phi_{r,n} \hat{x}_{r,k-1} + \Gamma_{r,n} u_{k-1})], \quad (3)$$

where  $\Phi_{r,n}$  and  $\Gamma_{r,n}$  are respectively the nominal state transition and command matrices (i.e., the ones used in the design).  $\Phi_r$  and  $\Gamma_r$  are the real matrices.  $\xi_{x_{r,k}}$  and  $\eta_k$  are Gaussian random variables associated to the system and measures, respectively, having a key role in the AOB design. Defining the estimation error as

$$e_{r,k} = x_{r,k} - \hat{x}_{r,k}, \quad (4)$$

and considering ideal conditions (i.e., the nominal matrices are equal to the real ones and  $\xi_{x_{r,k}}$  and  $\eta_k$  are zero),  $e_{r,k}$  can be computed from (1) and (3). Its value is

$$e_{r,k} = (\Phi_r - K_k C_r \Phi_r) e_{r,k-1}. \quad (5)$$

The error dynamics given by the eigenvalues of  $(\Phi_r - K_k C_r \Phi_r)$  is function of the  $K_k$  gain. The Kalman observer computes the best  $K_k$  in a straightforward way, minimizing the mean square error of the state estimate due to the random sources  $\xi_{x_{r,k}}$  and  $\eta_k$ . When there are unmodeled terms, (5) needs to be changed. A deterministic description of  $e_{r,k}$  is difficult, particularly when unknown modeling errors exist. Hence, a stochastic approach is attempted to describe it. If state feedback from the observer is used to control the system,  $p_k$  enters as an additional input

$$p_k = L_r e_{r,k}, \quad (6)$$

where  $L_r$  is the state feedback gain. A state space equation should be found to characterize this undesired input, leading the system to an extended state representation. Figure 1 shows the AOB.

To be able to track functions with unknown dynamics, a stochastic equation is used to describe  $p_k$

$$p_k - p_{k-1} = \xi_{p_k}, \quad (7)$$

in which  $\xi_{p_k}$  is a zero-mean Gaussian random variable<sup>1</sup>. Equation (7) says that the first derivative (or first-order evolution) of  $p_k$  is randomly distributed. Defining  ${}^N \xi_{p_k}$  as the  $N^{\text{th}}$ -order evolution of  $\xi_{p_k}$  (or the  $(N+1)^{\text{th}}$  order evolution of  $p_k$ ),

$${}^N \xi_{p_k} = {}^{N-1} \xi_{p_k} - {}^{N-1} \xi_{p_{k-1}}, \quad \text{with } {}^0 \xi_{p_k} = \xi_{p_k}, \quad (8)$$

the general form of (7) is

<sup>1</sup> The mathematical notation along the paper is for single input systems. For multiple input systems,  $p_k$  in (7) is a column vector with dimension equal to the number of inputs.

$$p_k = \sum_{j=1}^N (-1)^{j+1} \frac{N!}{j!(N-j)!} p_{k-j} + {}^{N-1}\xi_{p_k}. \quad (9)$$

$\{p_n\}$  is an AR process<sup>2</sup> of order  $N$  with undetermined mean. It has fixed parameters given by (9) and is driven by the statistics of  $\{{}^{N-1}\xi_{p_n}\}$ . The properties of  ${}^{N-1}\xi_{p_k}$  can change on-line based on a given strategy. The stochastic equation (7) for the AOB-1 or (9) for the AOB-N is used to describe  $p_k$ . If  ${}^{N-1}\xi_{p_k} = 0$ , (9) is a deterministic model for any disturbance  $p_k$  that has its  $N^{\text{th}}$ -derivative equal to zero. In this way, the stochastic information present in  ${}^{N-1}\xi_{p_k}$  gives more flexibility to  $p_k$ , since its evolutionary model is not rigid. The estimation of unknown functions using (7) and (9) is discussed in [Cortês et al., 2004].

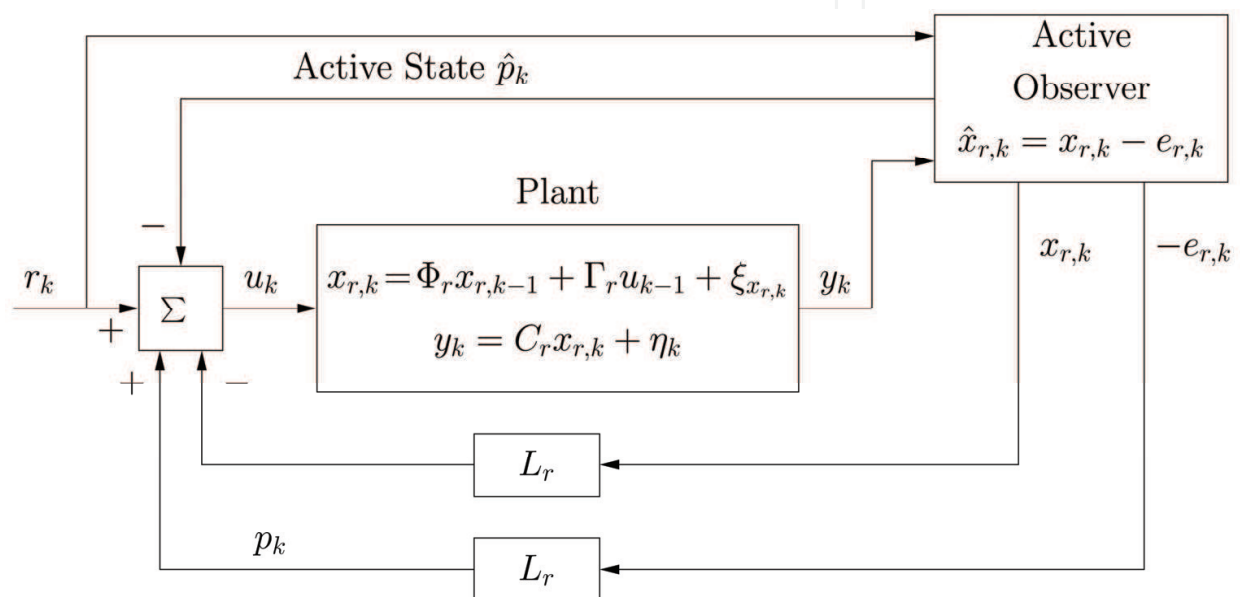


Figure 1. Active Observer. The active state  $\hat{p}_k$  compensates the error input, which is described by  $p_k$

## 5 AOB-1 Design

The AOB-1 algorithm is introduced in this section based on a continuous state space description of the system.

### 5.1 System Plant

Discretizing the system plant (without considering disturbances)

$$\begin{cases} \frac{dx_r(t)}{dt} = Ax_r(t) + Bu(t - \tau) \\ y(t) = C_r x_r(t) \end{cases} \quad (10)$$

with sampling time  $h$  and dead-time

$$\tau = (d - 1)h + \tau', \quad \text{with } 0 < \tau' \leq h, \quad (11)$$

<sup>2</sup>  $p_k$  is a random variable and  $\{p_n\}$  is a random process.

the discrete time system

$$\begin{bmatrix} x'_k \\ u_{k-d} \\ \vdots \\ u_{k-2} \\ u_{k-1} \end{bmatrix} = \begin{bmatrix} \Phi_1 & \Gamma_1 & \Gamma_0 & \cdots & 0 \\ 0 & 0 & 1 & \cdots & 0 \\ \vdots & \vdots & \vdots & \ddots & \vdots \\ 0 & 0 & 0 & \cdots & 1 \\ 0 & 0 & 0 & \cdots & 0 \end{bmatrix} \begin{bmatrix} x'_{k-1} \\ u_{k-d-1} \\ \vdots \\ u_{k-3} \\ u_{k-2} \end{bmatrix} + \begin{bmatrix} 0 \\ 0 \\ \vdots \\ 0 \\ 1 \end{bmatrix} u_{k-1} \tag{12}$$

and

$$y_k = C_r x_{r,k} \tag{13}$$

is obtained  $\Phi_1, \Gamma_0$  and  $\Gamma_1$  are given by (14) to (16), respectively [Aström & Wittenmark, 1997].

$$\Phi_1 = e^{Ah} = \phi(h), \tag{14}$$

$$\Gamma_0 = \int_0^{h-\tau'} \phi(\lambda) d\lambda B \tag{15}$$

and

$$\Gamma_1 = \phi(h - \tau') \int_0^{\tau'} \phi(\lambda) d\lambda B. \tag{16}$$

The state  $x_{r,k}$  is

$$x_{r,k} = [ x'_k \quad u_{k-d} \quad \cdots \quad u_{k-2} \quad u_{k-1} ]^T, \tag{17}$$

in which  $x'_k$  is the system state considering no dead-time. Therefore, the  $\tau$  of (6.10) increases the system order.

### 5.2 AOB-1 Algorithm

From Figure 1 and knowing (1) and (7), the augmented state space representation (open loop)<sup>3</sup> is

$$\begin{bmatrix} x_{r,k} \\ p_k \end{bmatrix} = \begin{bmatrix} \Phi_r & \Gamma_r \\ 0 & 1 \end{bmatrix} \begin{bmatrix} x_{r,k-1} \\ p_{k-1} \end{bmatrix} + \begin{bmatrix} \Gamma_r \\ 0 \end{bmatrix} u'_{k-1} + \begin{bmatrix} \xi_{x_{r,k}} \\ \xi_{p_k} \end{bmatrix} \tag{18}$$

where

$$u'_{k-1} = r_{k-1} - [ L_r \quad 1 ] \begin{bmatrix} x_{r,k-1} \\ \hat{p}_{k-1} \end{bmatrix}, \tag{19}$$

<sup>3</sup> In this context, open loop means that the state transition matrix does not consider the influence of state feedback.

$$\Phi_r = \begin{bmatrix} \Phi_1 & \Gamma_1 & \Gamma_0 & \cdots & 0 \\ 0 & 0 & 1 & \cdots & 0 \\ \vdots & \vdots & \vdots & \ddots & \vdots \\ 0 & 0 & 0 & \cdots & 1 \\ 0 & 0 & 0 & \cdots & 0 \end{bmatrix} \quad (20)$$

and

$$\Gamma_r = [0 \ 0 \ \cdots \ 0 \ 1]^T. \quad (21)$$

$L_r$  is obtained by any control technique applied to (12) to achieve a desired closed loop behavior. The measurement equation is

$$y_k = C \begin{bmatrix} x_{r,k} \\ p_k \end{bmatrix} + \eta_k, \quad (22)$$

with<sup>4</sup>

$$C = [C_r \ 0]. \quad (23)$$

The desired closed loop system appears when  $\hat{p}_k = p_k$  i.e.,

$$\begin{bmatrix} x_{r,k} \\ p_k \end{bmatrix} = \begin{bmatrix} \Phi_r - \Gamma_r L_r & 0 \\ 0 & 1 \end{bmatrix} \begin{bmatrix} x_{r,k-1} \\ p_{k-1} \end{bmatrix} + \begin{bmatrix} \Gamma_r \\ 0 \end{bmatrix} r_{k-1} + \begin{bmatrix} \xi_{x_{r,k}} \\ \xi_{p_k} \end{bmatrix}. \quad (24)$$

The state  $x_{r,k}$  in (24) is accurate if most of the modeling errors are merged to  $p_k$ . Hence,  $\xi_{x_{r,k}}$  should be small compared to  $\xi_{p_k}$ . The state estimation<sup>5</sup> must consider not only the influence of the uncertainty  $\xi_{x_{r,k}}$ , but also the deterministic term due to the reference input, the extended state representation and the desired closed loop response. It is given by<sup>6</sup>

$$\begin{bmatrix} \hat{x}_{r,k} \\ \hat{p}_k \end{bmatrix} = \begin{bmatrix} \Phi_{r,n} - \Gamma_{r,n} L_r & 0 \\ 0 & 1 \end{bmatrix} \begin{bmatrix} \hat{x}_{r,k-1} \\ \hat{p}_{k-1} \end{bmatrix} + \begin{bmatrix} \Gamma_{r,n} \\ 0 \end{bmatrix} r_{k-1} + \\ + K_k \left\{ y_k - C \left( \begin{bmatrix} \Phi_{r,n} - \Gamma_{r,n} L_r & 0 \\ 0 & 1 \end{bmatrix} \begin{bmatrix} \hat{x}_{r,k-1} \\ \hat{p}_{k-1} \end{bmatrix} + \begin{bmatrix} \Gamma_{r,n} \\ 0 \end{bmatrix} r_{k-1} \right) \right\}. \quad (25)$$

$K_k$  is

$$K_k = P_{1k} C^T [C P_{1k} C^T + R_k]^{-1}, \quad (26)$$

and

$$P_{1k} = \Phi_n P_{k-1} \Phi_n^T + Q_k, \quad (27)$$

<sup>4</sup> The form of  $C$  is maintained for the AOB-N, since the augmented states that describe  $p_k$  are not measured.

<sup>5</sup> The CKF algorithm can be seen in [Bozic, 1979].

<sup>6</sup>  $\Phi_{r,n}$  and  $\Gamma_{r,n}$  represent the nominal values of  $\Phi_{r,n}$  and  $\Gamma_{r,n}$ , respectively.

with

$$P_k = P_{1k} - K_k C P_{1k}. \quad (28)$$

$\Phi_n$  is the augmented open loop matrix used in the design,

$$\Phi_n = \begin{bmatrix} \Phi_{r,n} & \Gamma_{r,n} \\ 0 & 1 \end{bmatrix}. \quad (29)$$

$Q_k$  is the system noise matrix,<sup>7</sup>

$$Q_k = \begin{bmatrix} Q_{x_{r,k}} & 0 \\ 0 & Q_{p_k} \end{bmatrix}. \quad (30)$$

$R_k$  is the measurement noise matrix,  $R_k = E \{ \eta_k \eta_k^T \}$ .  $P_k$  is the mean square error matrix. It should be pointed out that  $P_{1k}$  given by (6.27) uses  $\Phi_n$ . More details can be seen in [Cortês, 2007].

## 6. AOB-N Design

The AOB-N is discussed in this section enabling stronger nonlinearities to be compensated by  $\hat{p}_k$ . Section 6.6.1 presents the AOB-N algorithm and Section 6.2 discusses the stochastic structure of AOB matrices.

### 6.1 AOB-N Algorithm

The AOB-1 algorithm has to be slightly changed for the AOB-N. Only the equation of the active state changes, entailing minor modifications in the overall AOB design. Equation (9) has the following state space representation:

$$\begin{bmatrix} p_{k-(N-1)} \\ p_{k-(N-2)} \\ \vdots \\ p_{k-1} \\ p_k \end{bmatrix} = \begin{bmatrix} 0 & 1 & 0 & \cdots & 0 \\ 0 & 0 & 1 & \cdots & 0 \\ \vdots & \vdots & \vdots & \ddots & \vdots \\ 0 & 0 & 0 & \cdots & 1 \\ a_N & a_{N-1} & a_{N-2} & \cdots & a_1 \end{bmatrix} \begin{bmatrix} p_{k-N} \\ p_{k-(N-1)} \\ \vdots \\ p_{k-2} \\ p_{k-1} \end{bmatrix} + \begin{bmatrix} 0 \\ 0 \\ \vdots \\ 0 \\ \xi_{p_k} \end{bmatrix}, \quad \text{with } a_i = (-1)^{i+1} \frac{N!}{i!(N-i)!}, \quad i = 1, \dots, N. \quad (31)$$

In compact form, (31) is represented by

$${}^N p_k = \Phi_{2,2} {}^N p_{k-1} + \xi_{N p_k}. \quad (32)$$

<sup>7</sup> Further analysis of the  $Q_k$  matrix is given in Section 6.2.

Equation (18) is now re-written as

$$\begin{bmatrix} x_{r,k} \\ {}^N p_k \end{bmatrix} = \begin{bmatrix} \Phi_r & \Phi_{1,2} \\ 0 & \Phi_{2,2} \end{bmatrix} \begin{bmatrix} x_{r,k-1} \\ {}^N p_{k-1} \end{bmatrix} + \begin{bmatrix} \Gamma_r \\ 0 \end{bmatrix} u'_{k-1} + \begin{bmatrix} \xi_{x_{r,k}} \\ \xi_{N p_k} \end{bmatrix}, \quad (33)$$

where

$${}^N p_k = [ p_{k-(N-1)} \quad p_{k-(N-2)} \quad \cdots \quad p_{k-1} \quad p_k ]^T. \quad (34)$$

$\Phi_{2,2}$  is the state transition matrix of (31),

$$\Phi_{1,2} = \begin{bmatrix} 0 & \cdots & 0 \\ \vdots & \ddots & \vdots \\ 0 & \cdots & 1 \end{bmatrix} \quad (35)$$

and

$$\xi_{N p_k} = [ 0 \quad 0 \quad \cdots \quad 0 \quad N^{-1} \xi_{p_k} ]^T. \quad (36)$$

The desired closed loop of (24) is changed to

$$\begin{bmatrix} x_{r,k} \\ {}^N p_k \end{bmatrix} = \begin{bmatrix} \Phi_L & 0 \\ 0 & \Phi_{2,2} \end{bmatrix} \begin{bmatrix} x_{r,k-1} \\ {}^N p_{k-1} \end{bmatrix} + \begin{bmatrix} \Gamma_r \\ 0 \end{bmatrix} r_{k-1} + \begin{bmatrix} \xi_{x_{r,k}} \\ \xi_{N p_k} \end{bmatrix}, \quad (37)$$

with

$$\Phi_L = \begin{bmatrix} \Phi_1 & \Gamma_1 & \Gamma_0 & \cdots & 0 \\ 0 & 0 & 1 & \cdots & 0 \\ \vdots & \vdots & \vdots & \ddots & \vdots \\ 0 & 0 & 0 & \cdots & 1 \\ -L_1 & -L_2 & -L_3 & \cdots & -L_M \end{bmatrix}. \quad (38)$$

The  $L_r$  components ( $L_1, \dots, L_M$ ) can be obtained by Ackermann's formula, i.e.,

$$L_r = [ 0 \quad \cdots \quad 0 \quad 1 ] W_c^{-1} P(\Phi_r). \quad (39)$$

$W_c$  is the reachability matrix

$$W_c = [ \Gamma_r \quad \Phi_r \Gamma_r \quad \cdots \quad \Phi_r^{M-1} \Gamma_r ], \quad (40)$$

and  $P(\Phi_r)$  is the desired characteristic polynomial. The state estimation is<sup>8</sup>

<sup>8</sup>  $\Phi_{L,n}$  is the nominal value of  $\Phi_L$

$$\begin{bmatrix} \hat{x}_{r,k} \\ {}^N\hat{p}_k \end{bmatrix} = \begin{bmatrix} \Phi_{L,n} & 0 \\ 0 & \Phi_{2,2} \end{bmatrix} \begin{bmatrix} \hat{x}_{r,k-1} \\ {}^N\hat{p}_{k-1} \end{bmatrix} + \begin{bmatrix} \Gamma_{r,n} \\ 0 \end{bmatrix} r_{k-1} \\ + K_k \left\{ y_k - C \left( \begin{bmatrix} \Phi_{L,n} & 0 \\ 0 & \Phi_{2,2} \end{bmatrix} \begin{bmatrix} \hat{x}_{r,k-1} \\ {}^N\hat{p}_{k-1} \end{bmatrix} + \begin{bmatrix} \Gamma_{r,n} \\ 0 \end{bmatrix} r_{k-1} \right) \right\}. \quad (41)$$

$K_k$  is given by (26) to (28), with

$$\Phi_n = \begin{bmatrix} \Phi_{r,n} & \Phi_{1,2} \\ 0 & \Phi_{2,2} \end{bmatrix}. \quad (42)$$

The state feedback gain  $L$  is

$$L = [ L_r \quad L_{Np_k} ], \quad (43)$$

with

$$L_{Np_k} = [ 0 \quad \dots \quad 0 \quad 1 ]. \quad (44)$$

## 6.2 AOB-N Matrices

$R_k$  is function of sensor characteristics. The form of  $Q_k$  is

$$Q_k = \begin{bmatrix} Q_{x_{r,k}} & 0 \\ 0 & Q_{Np_k} \end{bmatrix}. \quad (45)$$

$Q_{x_{r,k}}$  is a diagonal matrix. The uncertainty associated with  $x_{r,k}$  is low since all system disturbances should be compensated with  ${}^Np_k$ . Hence,  $Q_{x_{r,k}}$  should have low values compared to  $Q_{Np_k}$ , which is defined as

$$Q_{Np_k} = E \left\{ \xi_{Np_k} \cdot \xi_{Np_k}^T \right\}. \quad (46)$$

From (36),

$$Q_{Np_k} = \begin{bmatrix} 0 & \dots & 0 \\ \vdots & \ddots & \vdots \\ 0 & \dots & \sigma_{N-1}^2 \xi_{p_k} \end{bmatrix}. \quad (47)$$

$\sigma_{N-1}^2 \xi_{p_k}$  represents the variance of the  $(N-1)^{\text{th}}$  derivative of  $p_k$ , and is related with  $\sigma_{\xi_{p_k}}^2$ . Hence, the design can be done for  $\sigma_{\xi_{p_k}}^2$  (see [Cortês, 2007]).

## 6.3 AOB Estimation Strategies

An important property of the Kalman gain is introduced in Proposition 1, enabling to define different estimation strategies.

**Proposition 1** *The Kalman gain  $K_k$  obtained from (26) to (28) does not have a unique solution.*

*Proof:* Using (27) and (28), the matrix  $P_k$  can be written in a recursive way as

$$P_k = (I - K_k C_a)(\Phi_a P_{k-1} \Phi_a^T + Q_k). \quad (48)$$

Let's consider one solution

$$(Q_k, R_k, P_0) \rightarrow (K_k, P_k). \quad (49)$$

Another candidate solution

$$(Q'_k, R'_k, P'_0) \rightarrow (K_k, P'_k) \quad (50)$$

should be found, giving the same  $K_k$  values. If

$$Q'_k = \alpha Q_k, \quad (51)$$

in which  $\alpha$  is a scalar<sup>9</sup>, (48) is satisfied if

$$P'_k = \alpha P_k \text{ and } P'_{k-1} = \alpha P_{k-1}. \quad (52)$$

Hence, from (27), (51) and (52),

$$P'_{1k} = \alpha P_{1k}. \quad (53)$$

From (26), the new Kalman gain  $K'_k$  is

$$\begin{aligned} K'_k &= P'_{1k} C_a^T [C_a P'_{1k} C_a^T + R'_k]^{-1} \\ &= \alpha P_{1k} C_a^T [C_a \alpha P_{1k} C_a^T + R'_k]^{-1}. \end{aligned} \quad (54)$$

To accomplish  $K'_k = K_k$ , it is necessary that  $R'_k = \alpha R_k$ . The candidate solution exists and is

$$(Q'_k = \alpha Q_k, R'_k = \alpha R_k, P'_0 = \alpha P_0) \rightarrow (K_k, P'_k = \alpha P_k). \quad (55)$$

**Corollary 1** *What defines the Kalman gain, or the estimation strategy, are only the relations between the  $Q_k$  values, the  $R_k$  values, and both  $Q_k$  and  $R_k$  values.*

*Proof:* Similar to Proposition 1. •

In the AOB, the relations between the  $Q_k$  values are straightforward. The estimation strategy is thus based on the relation between  $Q_k$  and  $R_k$ . If model accuracy is very good compared with measure accuracy, a model based approach (MBA) is followed. The estimation  $\hat{x}_k$  given by (6.41) is mainly based on the model, giving little importance to measures. The Kalman gain has low values. On the other hand, if the measures are very accurate with respect to the model, a sensor based approach (SBA) is followed. The estimates are very sensitive to measures. The Kalman gain has high values. The hybrid based approach (HBA) is the general form of the AOB and establishes a trade-off between the SBA and MBA, i.e. it balances the estimates based on sensory and model information. To keep the same strategy as the AOB order changes, some adjustments in  $Q_k$  or  $R_k$  may be necessary, since the extended system matrix  $\Phi_a$  that affects  $K_k$  changes.

<sup>9</sup> Physically, it makes no sense a negative value of  $\alpha$ .

Eliminating the active state and redesigning  $Q$  (with new values) gives the CKF. In this situation, the  $Q$  design is not straightforward. Nevertheless, the relation between  $Q$  and  $R$  defines the control strategy.

For complex control tasks (e.g. compliant motion control), switching between AOB and CKF may appear dynamically as a function of the task state.

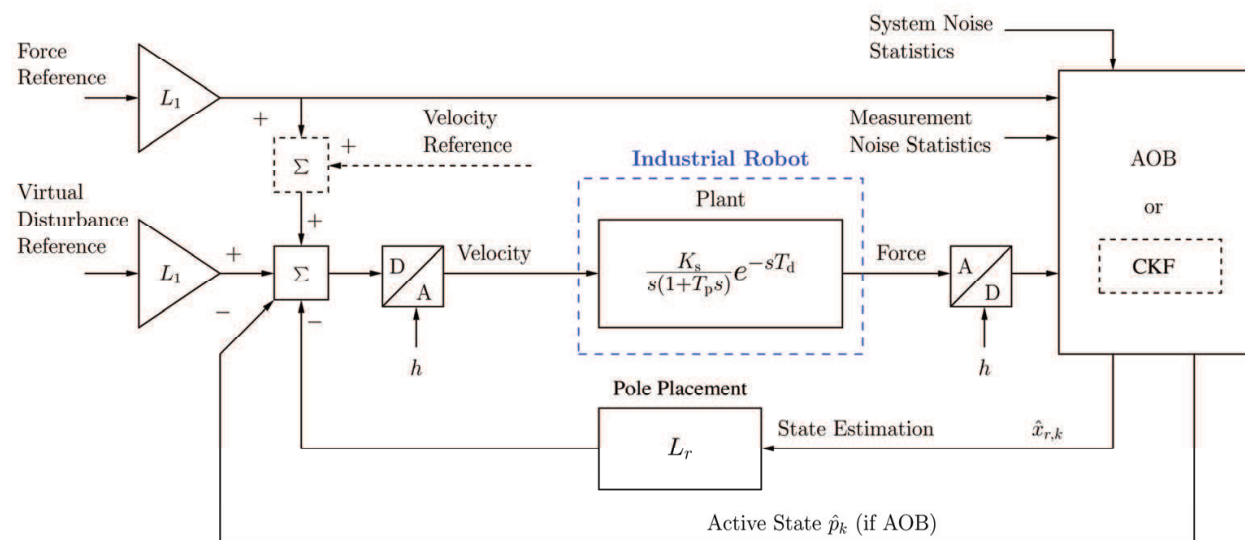


Figure 2. Global control scheme for each force/velocity dimension.  $K_s$  is the system stiffness.  $T_p$  is the position response time constant, and  $T_d$  is the system time delay due to the signal processing of the cascade controller

## 7. Experiments

If a manipulator is working in free space, position or velocity control of the end-effector is sufficient. For constrained motion, specialized control techniques have to be applied to cope with natural and artificial constraints. The experiments reported in this section apply AOBs to design a compliant motion controller (CMC) for the peg-in-hole task, guaranteeing model reinforcement in critical directions.

### 7.1 Peg-in-Hole Task

The robotic peg-in-hole insertion is one of the most studied assembly tasks. This longstanding problem has had many different solutions along the years. If the peg-hole clearance is big, position controlled robots can perform the task relatively easy. Otherwise, force control is necessary. The insertion requires position and angular constrained motion, which is a common situation in automation tasks. Several authors have tackled the peg-in-hole problem. Yoshimi and Allen [Yoshimi & Allen, 1994] performed the peg-in-hole alignment using uncalibrated cameras. Broenink and Tiernego [Broenink & Tiernego, 1996] applied impedance control methods to peg-in-hole assembly. Itabashi and co-authors [Itabashi et al., 1998] modeled the impedance parameters of a human based peg-in-hole insertion with hidden Markov models to perform a robotic peg-in-hole task. In [Morel et al., 1998], the peg-in-hole task is done combining vision and force control, and in [Kim et al., 2000], stiffness analysis is made for peg-in/out-hole tasks, showing the importance of the

compliance center location. Newman and co-authors [Newman et al., 2001] used a feature based technique to interpret sensory data, applying it to the peg-in-hole task.

Parameter	Value
$T_p$	0.032 [s]
$T_d$	0.040 [s]
$h$	0.008 [s]
$K_w$	3 [N/mm] (x lin.)
	3 [N/mm] (y lin.)
	20 [N/mm] (z lin.)
	100 [Nm/rad] (x rot.)
	100 [Nm/rad] (y rot.)

Table 1. Technology parameters of the Manutec R2 robot. Stiffness data

In our setup, the robotic peg-in-hole task is performed with an AOB based CMC. Figure 6.2 represents the CMC for each force dimension. The main goal is the human-robot skill transfer of the peg-in-hole task. The task is previously performed by a human, where the forces, torques and velocities of the peg are recorded as a function of its pose, using a teaching device. The robot should be able to perform the same task in a robust way after the skill transfer [Cortês et al., 2004]. The CMC is an important part of the system, since it tries to accomplish a desired compliant motion for a given geometric information. This CMC may change on-line between full AOB, CKF or "pure" state feedback, based on the task state. If velocity signals are dominant, the CKF should be used since the full AOB annihilates any external inputs. If force signals are dominant, the full AOB is a good choice. Hence, the CMC can easily handle two reference inputs,  $f_d$  (force) and  $v_d$  (velocity). The natural constraints imply complementarity of the reference signals. When  $f_d$  is different than zero  $v_d$  is almost zero and vice-versa. In the sequel, the performance of the 6 DOF peg-in-hole task is analyzed with the AOB and CKF in the loop.

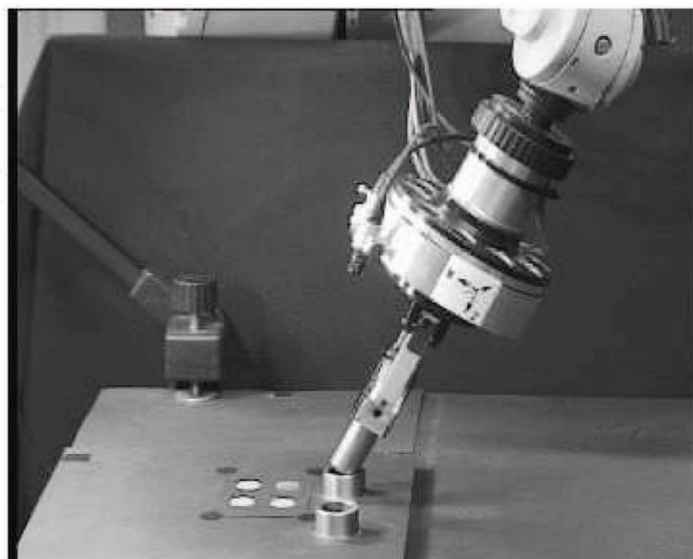
## 7.2 Experimental Setup

Experimental tests have been done in a robotic testbed at DLR (German Aerospace Center). The main components of this system are:

- A Manutec R2 industrial robot with a Cartesian position interface running at 8 [ms] and an input dead-time of 5 samples, equivalent to 40 [ms].
- A DLR end-effector, which consists of a compliant force/torque sensor providing force/torque measurements every 8 [ms]. The technology data of the robot and the force sensor stiffness are summarized in Table 6.1. The manipulator compliance is lumped in the force sensor.
- A multi-processor host computer running UNIX, enabling to compute the controller at each time step.
- Two cameras for stereo vision are mounted on the end-effector. A pneumatic gripper holds a steel peg of 30 [mm] length and of 23 [mm] diameter. The peg-hole has a clearance of 50 [ $\mu$ m], which corresponds to a tolerance with ISO quality 9. The hole is

chamferless. The environment is very stiff ( $K_s \approx K_w$ ). Vision and pose sense belong to the data fusion architecture (see [Cortês et al., 2004]).

- A picture of the experimental setup is depicted in Figure 3. Figure 3.a represents the peg-in-hole task with a three point contact. Figure 3.b shows the task execution with human interference.



(a)



(b)

Figure 3. Experimental setup, (a) Manutec R2 robot ready to perform the peg-in-hole task, (b) Human interaction during the peg-in-hole task

### 7.3 AOB Matrices

This section discusses the AOB design for the CMC controller.

#### System Plant Matrices

For each DOF, the position response of the Manutec R2 robot is

$$G_p(s) = \frac{1}{1 + T_p s} e^{-sT_d}. \quad (56)$$

Inserting the system stiffness  $K_s$ , the system plant can be written as

$$G(s) = \frac{k_1}{s(s + p_1)} e^{-st_d}, \quad (57)$$

with

$$k_1 = K_s/T_p, \quad p_1 = 1/T_p \quad \text{and} \quad t_d = T_d. \quad (58)$$

Its equivalent temporal representation is

$$\ddot{y} + p_1 \dot{y} = k_1 u(t - t_d), \quad (59)$$

where  $y$  is the plant output (force) and  $u$  is the plant input (velocity). Defining the state variables as

$$x_1 = y \quad \text{and} \quad x_2 = \dot{y}, \quad (60)$$

the state space description of (59) is given by

$$\begin{bmatrix} \dot{x}_1 \\ \dot{x}_2 \end{bmatrix} = \begin{bmatrix} 0 & 1 \\ 0 & -p_1 \end{bmatrix} \begin{bmatrix} x_1 \\ x_2 \end{bmatrix} + \begin{bmatrix} 0 \\ k_1 \end{bmatrix} u(t - t_d). \quad (61)$$

Physically,  $x_1$  represents the force at the robot's end effector and  $x_2$  is the force derivative. Knowing (61), the AOB design described in Sections 5 and 6 can be applied in straightforward way.

#### Stochastic Matrices

For the first dimension  $f_x$ ,

$$Q_k(f_x) = \begin{bmatrix} 10^{-12} & \dots & 0 & 0 \\ 0 & \dots & 0 & 0 \\ \vdots & \ddots & \vdots & \vdots \\ 0 & \dots & 10^{-12} & 0 \\ 0 & \dots & 0 & 10^{-5} \end{bmatrix}, \quad (62)$$

and

$$P_0(f_x) = \begin{bmatrix} 10^{-4} & 0 & \dots & 0 & 0 \\ 0 & 10^{-4} & \dots & 0 & 0 \\ \vdots & \vdots & \ddots & \vdots & \vdots \\ 0 & 0 & \dots & 10^{-4} & 0 \\ 0 & 0 & \dots & 0 & 10^{-4} \end{bmatrix}. \quad (63)$$

The value of  $R_k$  was obtained experimentally. It is given by

$$R_k(f_x) = 2.1 \times 10^{-2}. \quad (64)$$

For the second dimension  $f_y$ ,  $Q_k$  is

$$Q_k(f_y) = Q_k(f_x)R_k(f_y)/R_k(f_x), \tag{65}$$

$$P_0(f_y) = P_0(f_x)R_k(f_y)/R_k(f_x), \tag{66}$$

with

$$R_k(f_y) = 7.4 \times 10^{-4}. \tag{67}$$

Analogous equations are obtained for the other force/torque dimensions.

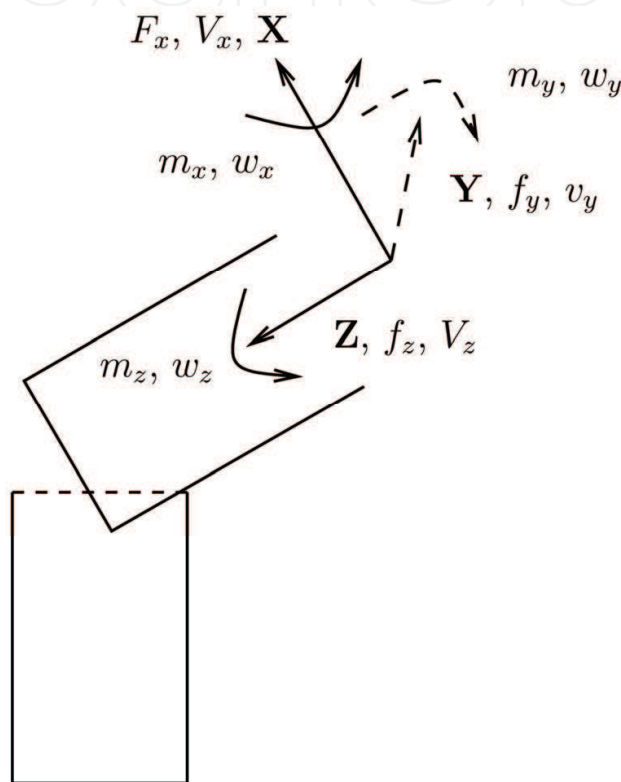


Figure 4. Peg-on-hole with a three point contact. Cartesian axes in peg coordinates. Representation of the forces and velocities (6 DOF).  $w_y$  represents the alignment velocity and  $v_z$  the insertion velocity

**Control Matrices**

The state feedback gain  $L_r$  is computed for a critically damped response with closed loop time constant  $\tau_c$  equal to

$$\tau_c = 10T_p. \tag{68}$$

The other poles due to dead-time are mapped in the  $z$ -domain at  $z = 0$  (discrete poles). The reachability matrix  $W_c$  and the characteristic polynomial are described in the AOB algorithm (see Sections 5 and 6).

## 7.4 Experimental Results

The execution of the peg-in-hole task starts with the peg-on-hole with a three point contact. The Cartesian axes and the corresponding forces and velocities are represented in Figure 6.4 in peg coordinates. If the peg is perfectly aligned, the angular velocity  $w_y$  (negative sign) aligns the peg in vertical position, while  $f_x$  (negative sign) and  $f_z$  (positive sign) guarantee always a three point contact during the alignment phase. Then, only the velocity  $v_z$  is needed to put the peg into the hole. Non-zero  $m_y$  and  $f_x$  reinforce contact with the hole inner surface during insertion. Ideally, the relevant signals for the alignment phase are  $f_x$ ,  $f_z$  and  $w_y$ , and for the insertion phase are  $v_z$ ,  $m_y$  and  $f_x$ . Figures 6.5 and 6.6 show force/velocity data<sup>10</sup> for the peg-in-hole task, applying different control strategies. An artificial neural network (ANN) trained with human data generates the desired compliant motion signals (velocity and force) from pose sense. Figures 5 and 6 present results when the AOB-1, HBA is applied to all directions except the  $z$  direction that has the CKF, SBA. The moment  $m_y$  is only function of the contact forces and of the contact geometry during the alignment phase [Koeppel, 2001]. Hence, the controller for  $m_y$  is only active during the insertion.  $f_x$ ,  $f_y$ ,  $m_y$ ,  $m_z$ , and the corresponding velocities  $v_x$ ,  $v_y$ ,  $w_y$  and  $w_z$  follow well the reference signals (Figures 5.a, 5.b, 5.e, 5.f and Figures 6.a, 6.b, 6.e, 6.f, respectively). There is a slight misalignment in the peg during the alignment phase which originates a moment  $m_x$  (Figure 5.d). The CMC reacts issuing an angular velocity  $w_x$  represented in Figure 6.d. The insertion velocity  $v_z$  is slightly biased during the alignment phase (Figure 6.c). These errors come from imperfect training of the ANN ([Cortês et al., 2004]). Therefore, the force  $f_z$  is seriously affected by  $v_z$  errors. The stiffness in  $z$  direction is high (Table 1), magnifying even more feedforward errors. An overshoot of almost 20 [N] is reached before insertion creating a barrier to the task execution speed due to force sensor limits (Figure 5.c). An error of 4 [N] in  $f_z$  (at the beginning of the alignment phase) is due to feedforward velocity errors (see Figures 5.c and 6.c.). Since no active control actions are done for the  $z$  dimension, the degradation of the control performance is evident, stressing the importance of AOB actions.

## 8. Conclusions

The first part of the chapter discusses model-reference adaptive control in the framework of Kalman active observers (AOBs). The second part addresses experiments with an industrial robot. Compliant motion control with AOBs is analyzed to perform the peg-in-hole task.

The AOB design is based on: 1) A desired closed loop system, corresponding to the reference model. 2) An extra equation (active state) to estimate an equivalent disturbance referred to the system input, providing a feedforward compensation action. The active state is modeled as an auto-regressive process of order  $N$  with fixed parameters (evolutions) driven by a Gaussian random source. 3) The stochastic design of the Kalman matrices ( $Q_k$  and  $R_k$ ) for the AOB context.  $Q_k$  has a well defined structure. Most of the modeling errors are merged in the active state, therefore, the model for the other states is very accurate (the reference model has low uncertainty). The relation between  $Q_k$  and  $R_k$  defines the estimation strategy, making the state estimates more or less sensitive to measures.

<sup>10</sup> The measured force/velocity signals were filtered off-line by a 6th order low-pass Butterworth filter with a 2 [Hz] cut-off frequency. The phase distortion was compensated.

Experiments with the peg-in-hole with tight clearance have shown the AOB importance in the control strategy. When there are relevant inconsistencies between force and velocity signals, non-active control techniques give poor results. For complex compliant motion tasks, on-line switching between AOB and classical Kalman filter (CKF) is easy, since the CKF is a particular form of the AOB which does not require extra computational power.

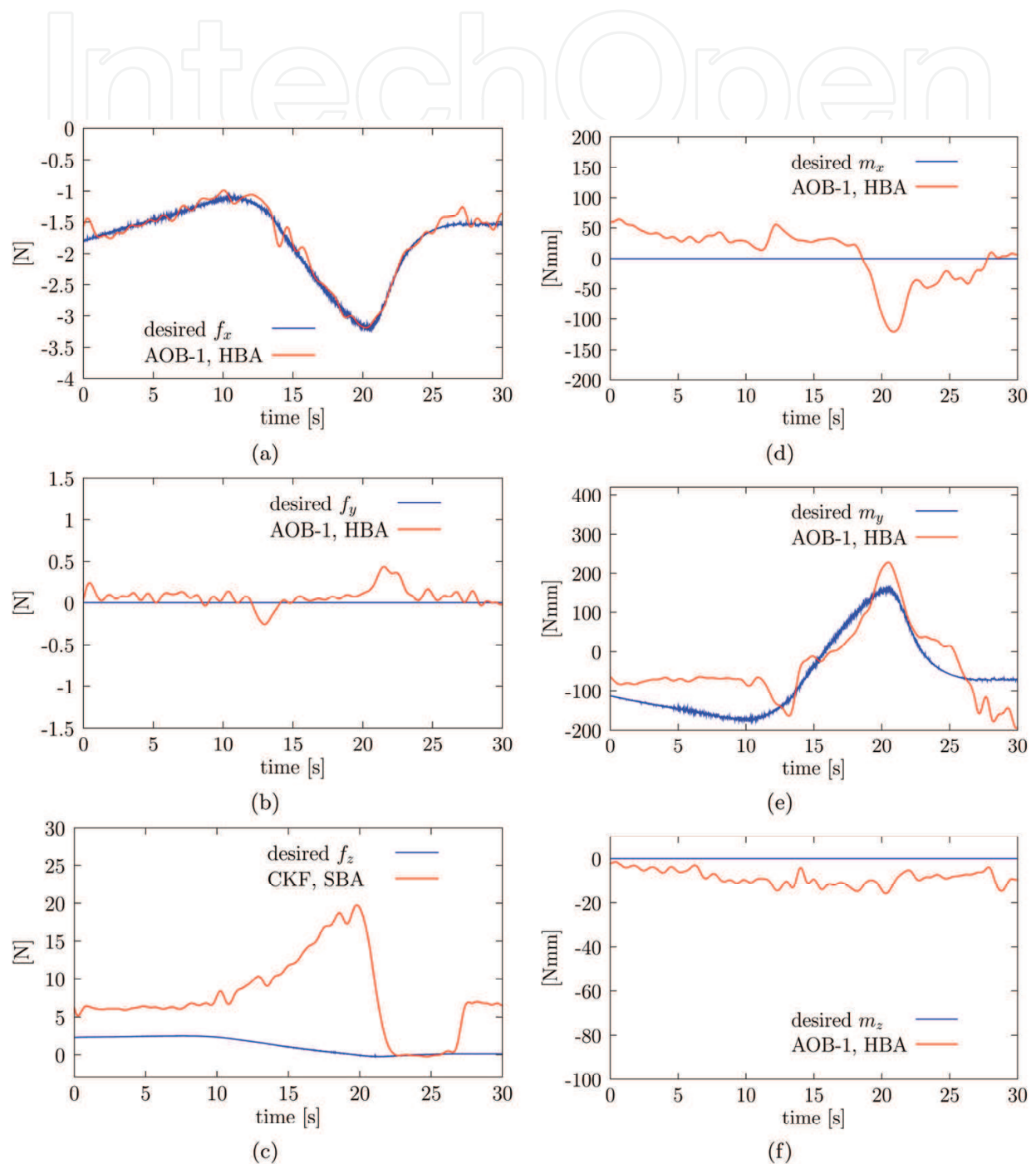


Figure 5. Experimental results for the peg-in-hole task with scale 10 (i.e. ten times slower than human demonstration). AOB-1, HBA vs. CKF, SBA. Force data.  $f_z$  always with CKF, SBA

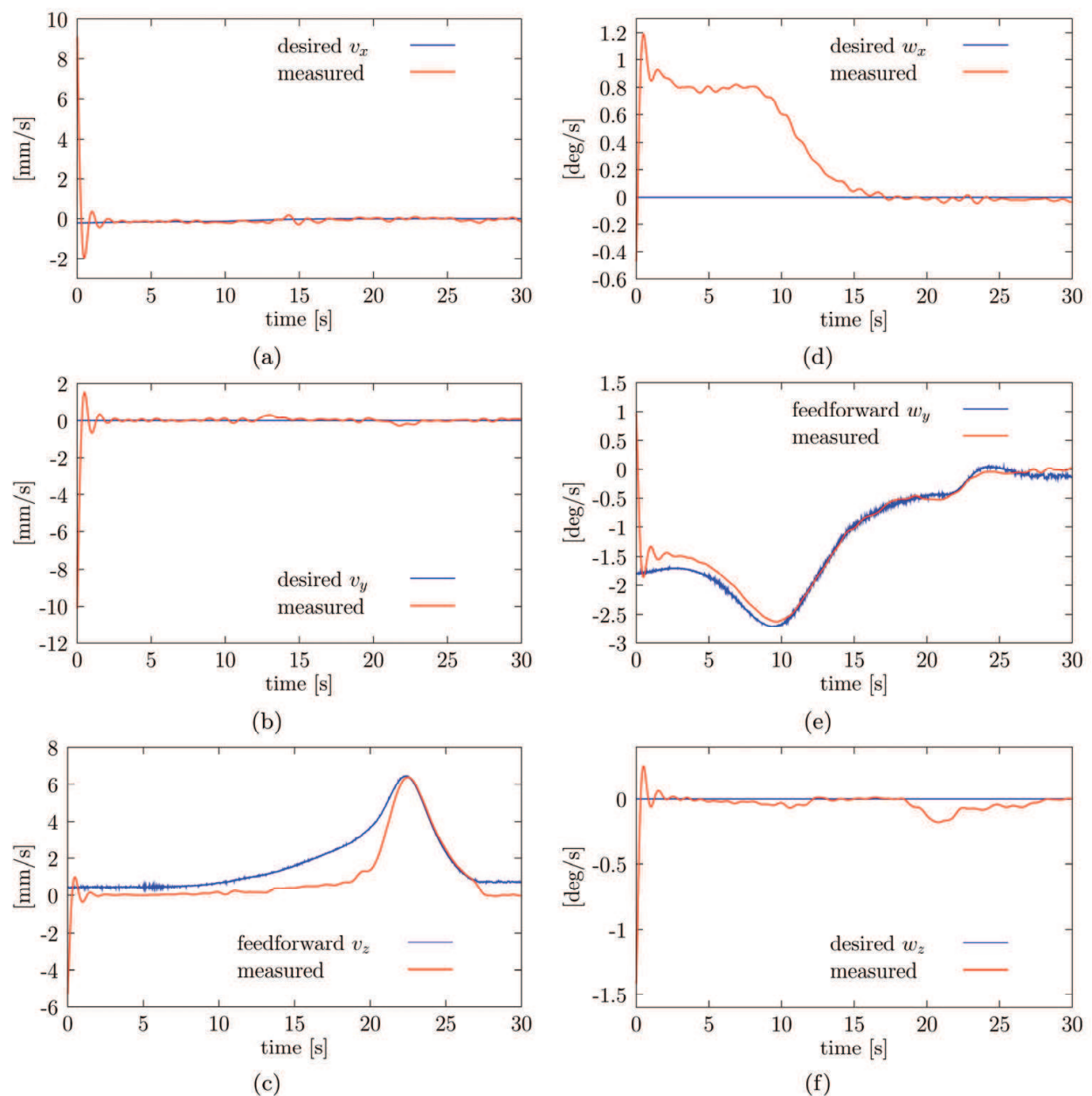


Figure 6. Experimental results for the peg-in-hole task with scale 10. AOB-1, HBA vs. CKF, SBA. Velocity data.  $f_z$  always with CKF, SBA

## 9. Acknowledgments

This work was supported in part by the Portuguese Science and Technology Foundation (FCT) Project PTDC/EEA-ACR/72253/2006.

## 10. References

Astrom, K. J. & Wittenmark, B. (1997). *Computer Controlled Systems: Theory and Design*. Prentice Hall. [Astrom & Wittenmark, 1997]

- Bajcinca, N., Cortesão, R. & Hauschild, M. (2005). *Autonomous Robots* 19, 193-214. [Bajcinca et al., 2005]
- Bozic, S. M. (1979). *Digital and Kalman Filtering*. Edward Arnold, London. [Bozic, 1979]
- Broenink, J. & Tierneho, M. (1996). In *Proc. of the European Simulation Symposium* pp. 504–509, Italy. [Broenink & Tierneho, 1996]
- Chen, B., Lin, Z. & Liu, K. (2002). *Automatica* 38, 293-299. [Chen et al., 2002]
- Chen, X., Komada, S. & Fukuda, T. (2000). *IEEE Transactions on Industrial Electronics* 47, 429-435. [Chen et al., 2000]
- Chu, D. & Mehrmann, V. (2000). *SIAM J. on Control and Optimization* 38, 1830-1858. [Chu & Mehrmann, 2000]
- Coelho, P. & Nunes, U. (2005). *IEEE Transactions on Robotics* 21, 252-261. [Coelho & Nunes, 2005]
- Commault, C., Dion, J. & Hovelaque, V. (1997). *Automatica* 33, 403-409. [Commault et al., 1997]
- Cortesão, R. (2007). *Int. J. of Intelligent and Robotic Systems* 48, 131-155. [Cortesão, 2007]
- Cortesão, R. & Bajcinca, N. (2004). In *Proc. of the Int. Conf. on Intelligent Robots and Systems (IROS)* pp. 1148-1153, Japan. [Cortesão & Bajcinca, 2004]
- Cortesão, R., Koeppe, R., Nunes, U. & Hirzinger, G. (2000). *Int. J. of Machine Intelligence and Robotic Control (MIROC)*. Special Issue on Force Control of Advanced Robotic Systems 2, 59-68. [Cortesão et al., 2000]
- Cortesão, R., Koeppe, R., Nunes, U. & Hirzinger, G. (2001). In *Proc. of the Int. Conf. on Intelligent Robots and Systems (IROS)* pp. 1876-1881, USA. [Cortesão et al., 2001]
- Cortesão, R., Koeppe, R., Nunes, U. & Hirzinger, G. (2004). *IEEE Transactions on Robotics* 20, 941-952. [Cortesão et al., 2004]
- Cortesão, R., Park, J. & Khatib, O. (2006). *IEEE Transactions on Robotics* 22, 987-999. [Cortesão et al., 2006]
- Doyle, J. (1978). *IEEE Transactions on Automatic Control* 23, 756-757. [Doyle, 1978]
- Doyle, J. & Stein, G. (1979). *IEEE Transactions on Automatic Control* 24, 607-611. [Doyle & Stein, 1979]
- Estrada, M. & Malabre, M. (1999). *IEEE Transactions on Automatic Control* 44, 1311-1315. [Estrada & Malabre, 1999]
- Itabashi, K., Hirana, K., Suzuki, T., Okuma, S. & Fujiwara, F. (1998). In *Proc. of the Int. Conf. on Robotics and Automation (ICRA)* pp. 1142-1147, Belgium. [Itabashi et al., 1998]
- Kim, B., Yi, B., Suh, I. & Oh, S. (2000). In *Proc. of the Int. Conf. on Intelligent Robots and Systems (IROS)* pp. 1229-1236, Japan. [Kim et al., 2000]
- Koeppe, R. (2001). Robot Compliant Motion Based on Human Skill. *PhD thesis*, ETH Zurich. [Koeppe, 2001]
- Maia, R., Cortesão, R., Nunes, U., Silva, V. & Fonseca, F. (2003). In *Proc. of the Int. Conf. on Advanced Robotics* pp. 876-882,, Portugal. [Maia et al., 2003]
- Morel, G., Malis, E. & Boudet, S. (1998). In *Proc. of the Int. Conf. on Robotics and Automation (ICRA)* pp. 1743-1748,, Belgium. [Morel et al., 1998]
- Newman, W., Zhao, Y. & Pao, Y. (2001). In *Proc. of the Int. Conf. on Robotics and Automation (ICRA)* pp. 571-576,, Belgium. [Newman et al., 2001]
- Oda, N. (2001). *J. of Robotics and Mechatronics* 13, 464-471. [Oda, 2001]
- Park, J., Cortesão, R. & Khatib, O. (2004). In *Proc. of the IEEE Int. Conf. on Robotics and Automation, (ICRA)* pp. 4789-4794,, USA. [Park et al., 2004]

- Park, J. & Khatib, O. (2005). In *Proc. of the Int. Conf. on Robotics and Automation (ICRA)* pp. 3624-3629, Spain. [Park & Khatib, 2005]
- Petersen, I., James, M. & Dupuis, P. (2000). *IEEE Transactions on Automatic Control* 45, 398-412. [Petersen et al., 2000]
- Safanov, M. & Athans, M. (1977). *IEEE Transactions on Automatic Control* 22, 173-179. [Safanov & Athans, 1977]
- Schutter, J. D. (1988). In *Proc. of the Int. Conf. on Robotics and Automation (ICRA)* pp. 1497-1502, USA. [Schutter, 1988]
- Yoshimi, B. & Allen, P. (1994). In *Proc. of the Int. Conf. on Robotics and Automation (ICRA)* vol. 4, pp. 156-161, USA. [Yoshimi & Allen, 1994]

IntechOpen



## **Frontiers in Adaptive Control**

Edited by Shuang Cong

ISBN 978-953-7619-43-5

Hard cover, 334 pages

**Publisher** InTech

**Published online** 01, January, 2009

**Published in print edition** January, 2009

The objective of this book is to provide an up-to-date and state-of-the-art coverage of diverse aspects related to adaptive control theory, methodologies and applications. These include various robust techniques, performance enhancement techniques, techniques with less a-priori knowledge, nonlinear adaptive control techniques and intelligent adaptive techniques. There are several themes in this book which instance both the maturity and the novelty of the general adaptive control. Each chapter is introduced by a brief preamble providing the background and objectives of subject matter. The experiment results are presented in considerable detail in order to facilitate the comprehension of the theoretical development, as well as to increase sensitivity of applications in practical problems

### **How to reference**

In order to correctly reference this scholarly work, feel free to copy and paste the following:

Rui Cortesao (2009). Model Reference Adaptive Control for Robotic Manipulation with Kalman Active Observers, *Frontiers in Adaptive Control*, Shuang Cong (Ed.), ISBN: 978-953-7619-43-5, InTech, Available from:

[http://www.intechopen.com/books/frontiers\\_in\\_adaptive\\_control/model\\_reference\\_adaptive\\_control\\_for\\_robotic\\_manipulation\\_with\\_kalman\\_active\\_observers](http://www.intechopen.com/books/frontiers_in_adaptive_control/model_reference_adaptive_control_for_robotic_manipulation_with_kalman_active_observers)

**INTECH**  
open science | open minds

### **InTech Europe**

University Campus STeP Ri  
Slavka Krautzeka 83/A  
51000 Rijeka, Croatia  
Phone: +385 (51) 770 447  
Fax: +385 (51) 686 166  
[www.intechopen.com](http://www.intechopen.com)

### **InTech China**

Unit 405, Office Block, Hotel Equatorial Shanghai  
No.65, Yan An Road (West), Shanghai, 200040, China  
中国上海市延安西路65号上海国际贵都大饭店办公楼405单元  
Phone: +86-21-62489820  
Fax: +86-21-62489821

© 2009 The Author(s). Licensee IntechOpen. This chapter is distributed under the terms of the [Creative Commons Attribution-NonCommercial-ShareAlike-3.0 License](#), which permits use, distribution and reproduction for non-commercial purposes, provided the original is properly cited and derivative works building on this content are distributed under the same license.

IntechOpen

IntechOpen